



**HAL**  
open science

## The importance of mass accuracy in selected ion monitoring analysis of branched and isoprenoid tetraethers

Nina Davtian, Edouard Bard, Guillemette Ménot, Yoann Fagault

► **To cite this version:**

Nina Davtian, Edouard Bard, Guillemette Ménot, Yoann Fagault. The importance of mass accuracy in selected ion monitoring analysis of branched and isoprenoid tetraethers. *Organic Geochemistry*, 2018, 118, pp.58 - 62. 10.1016/j.orggeochem.2018.01.007 . hal-01713879

**HAL Id: hal-01713879**

**<https://hal.science/hal-01713879>**

Submitted on 2 Feb 2024

**HAL** is a multi-disciplinary open access archive for the deposit and dissemination of scientific research documents, whether they are published or not. The documents may come from teaching and research institutions in France or abroad, or from public or private research centers.

L'archive ouverte pluridisciplinaire **HAL**, est destinée au dépôt et à la diffusion de documents scientifiques de niveau recherche, publiés ou non, émanant des établissements d'enseignement et de recherche français ou étrangers, des laboratoires publics ou privés.

1 The importance of mass accuracy in selected ion monitoring

2 analysis of branched and isoprenoid tetraethers

3 Nina Davtian <sup>a,\*</sup>, Edouard Bard <sup>a</sup>, Guillemette Ménot <sup>b</sup>, Yoann Fagault <sup>a</sup>

4

5 <sup>a</sup> CEREGE, Aix-Marseille Univ, CNRS, IRD, INRA, Collège de France, 13545

6 Aix-en-Provence, France

7 <sup>b</sup> Univ Lyon, ENS de Lyon, Université Lyon 1, CNRS, UMR 5276 LGL-TPE,

8 F-69364, Lyon, France

9

10

11 \*Corresponding author. *E-mail address*: [davtian@cerege.fr](mailto:davtian@cerege.fr) (N. Davtian)

12

13 **ABSTRACT**

14 Among the new proxies based on the distribution of glycerol dialkyl glycerol  
15 tetraethers (GDGTs), the BIT index (Branched and Isoprenoid Tetraether  
16 index) is one of the most difficult to determine accurately, as shown by two  
17 round-robin GDGT studies. Sensitivity to mass spectrometer settings and  
18 tuning, and a diversity of mass spectrometry techniques may explain the  
19 relatively large observed interlaboratory scatter. However, the mass defect  
20 difference between crenarchaeol and branched GDGTs (brGDGTs) has never  
21 been specifically scrutinized. In this study, we analyzed five sediment  
22 samples with contrasting BIT values using about 60  $m/z$  values to assess the  
23 shape of GDGT peaks using selected ion monitoring. We then assessed the  
24 biases on relative GDGT signals and mass spectrometry-derived BIT values  
25 under two scenarios which ignore the systematic mass defect difference  
26 between crenarchaeol and brGDGTs. Our results show that approximate  
27 mass selection for GDGT analysis using selected ion monitoring generates  
28 losses of relative GDGT signals of up to 36%. The observed effects on BIT  
29 values are maximal for intermediate BIT values, with shifts of BIT values of  
30  $\pm 0.1$  unit. The shifts of BIT values due to approximate mass selection are  
31 thus not negligible compared to the interlaboratory scatter evidenced by the  
32 latest round-robin GDGT study.

33

34 *Keywords:* Mass defect difference, selected ion monitoring, HPLC–APCI-MS,  
35 GDGTs, BIT index.

36

## 37 1. Introduction

38 The development of normal phase high performance liquid  
39 chromatography coupled to positive ion atmospheric pressure chemical  
40 ionization mass spectrometry (HPLC–APCI-MS) has greatly facilitated the  
41 analysis of polar lipids with high molecular weights (Hopmans et al., 2000).  
42 Following this analytical development, a number of new proxies based on  
43 the relative distributions of glycerol dialkyl glycerol tetraethers (GDGTs)  
44 have been developed (Schouten et al., 2013b and References therein).  
45 Among the new GDGT-based proxies, the BIT index (Branched and  
46 Isoprenoid Tetraether index; Hopmans et al., 2004) has been proposed as a  
47 tracer for terrestrial organic carbon in sediments. The BIT index is a ratio  
48 that compares the abundance of crenarchaeol, an isoprenoid GDGT  
49 produced by *Thaumarchaeota* (e.g., Sinninghe Damsté et al., 2002), with  
50 those of branched GDGTs (brGDGTs), which are produced by (acido)bacteria  
51 (Weijers et al., 2009; Sinninghe Damsté et al., 2011, 2014). It is noteworthy  
52 that the BIT index, while widely determined, needs to be carefully  
53 interpreted in order to reconstruct terrigenous fluxes (Schouten et al., 2013b  
54 and References therein).

55 The two international intercomparisons of GDGT measurements  
56 (round-robin) have shown specific difficulties associated with calculation of  
57 the BIT index (Schouten et al., 2009, 2013a). Escala et al. (2009) have shown  
58 that the BIT index, which considers two different families of GDGTs, is  
59 particularly sensitive to APCI conditions. Such sensitivity may explain part

60 of the relatively large interlaboratory scatter of the BIT index, especially for  
61 samples with intermediate BIT values (Schouten et al., 2009, 2013a).  
62 However, the approximate mass selection for GDGT analysis using selected  
63 ion monitoring (SIM) has not yet been explored as a reason for the poor  
64 reproducibility between labs of the BIT index. It is noteworthy that while  
65 many types of MS and GDGT analysis techniques exist, most laboratories  
66 analyzed GDGTs using SIM with single quadrupole mass spectrometers  
67 (QMS) during both round-robin GDGT studies (Schouten et al., 2009,  
68 2013a).

69       Following a review of about three hundred manuscripts where  
70 GDGTs were analyzed using SIM with QMS, we have found only a dozen  
71 manuscripts (ca. 4%) where  $m/z$  values are written with at least one decimal  
72 place (e.g., Herfort et al., 2006; Yang et al., 2011; Basse et al., 2014). In the  
73 other manuscripts, the  $m/z$  values are either systematically written as  
74 integer numbers (e.g., Cao et al., 2017; Freymond et al., 2017; Naafs et al.,  
75 2017), or not indicated at all (e.g., Keisling et al., 2017; Ruan et al., 2017;  
76 Woelders et al., 2017). This means that only a few manuscripts clearly  
77 reported exact  $m/z$  values rounded up to at least one decimal rather than  
78 approximate, integer  $m/z$  values for GDGT analysis using SIM.

79       In the present study, we analyzed five sediment samples with  
80 contrasting BIT values. We selected about 60  $m/z$  values for GDGT detection  
81 using SIM to obtain the relative GDGT signals depending on mass selection.  
82 We then assessed the biases on relative GDGT signals and on BIT values

83 under two scenarios that ignore the systematic mass defect difference  
84 between crenarchaeol and brGDGTs.

85

## 86 **2. Materials and methods**

87 The mass defect is defined as the exact molecular mass minus the  
88 nominal molecular mass – i.e., Mass defect =  $M_{\text{exact}} - M_{\text{nominal}}$ . GDGTs are  
89 long hydrogenated molecules and their mass defect values are around 1 or  
90 more. It should be noted that the mass defect is independent of the  
91 protonation – which adds about 1 Da to nominal and exact molecular  
92 masses. In this study, the assumption of a unique mass defect for all  
93 compounds is referred to as a “unique mass defect scenario”.

94 Taking into account the newest brGDGT isomers (De Jonge et al.,  
95 2013; Ding et al., 2016), the BIT index equation of Hopmans et al. (2004)  
96 has been redefined as follows:

$$\text{BIT} = \frac{\text{Ia} + \text{IIa}_5 + \text{IIIa}_5 + \text{IIa}_6 + \text{IIIa}_6 + \text{IIa}_7 + \text{IIIa}_7}{\text{Cren} + \text{Ia} + \text{IIa}_5 + \text{IIIa}_5 + \text{IIa}_6 + \text{IIIa}_6 + \text{IIa}_7 + \text{IIIa}_7} \quad (1)$$

97 Roman numerals refer to brGDGT isomers following the nomenclature of  
98 Ding et al. (2016). Equation (1) can be simplified as  $\text{BIT} = A/(A+B)$ , with A  
99 and B the brGDGTs and crenarchaeol, respectively. In addition, A and B are  
100 distinguished by their different mass defects (Table 1).

101 Five previously analyzed sediment samples with contrasting BIT  
102 values were selected: a modern marine sediment from the Bay of Marseille  
103 (Mediterranean Sea, 43.26°N, 5.29°E; about 60 m water depth), a modern  
104 lacustrine sediment from Lake Chad (LT17, 13°N, 14°E) and three sediment

105 samples from core MD04-2790. The core was retrieved from the continental  
106 shelf of the Black Sea (44.21°N, 30.99°E) during the ASSEMBLAGE 1 cruise  
107 of R.V. Marion Dufresne. The BIT values of the core and modern marine  
108 sediments were previously determined by Ménot and Bard (2012) and  
109 Sanchi et al. (2013), respectively. The lacustrine sediment LT17 and the  
110 marine sediment from the Bay of Marseille were selected and analyzed as  
111 in-house standard sediments to check the absence of instrumental drift in  
112 GDGT-derived indices.

113         New aliquots of the modern sediment samples were extracted at  
114 CEREGE with DCM:MeOH (9:1, v:v) using an accelerated solvent extractor  
115 ASE 350 (Dionex) at 120 °C and 10<sup>7</sup> Pa. Total lipid extracts were separated  
116 following the automated procedure established by Sanchi et al. (2013). The  
117 polar fractions of the five selected samples were then dissolved in  
118 hexane:isopropanol (98.2:1.8, v:v) prior to GDGT analysis on an Agilent  
119 1260 Infinity HPLC coupled to a 6120 single QMS installed at CEREGE.  
120 The GDGTs were separated using similar chromatographic columns and  
121 solvents to Hopmans et al. (2016), as well as the same elution program, but  
122 with a 24 min re-equilibration time.

123         The APCI source conditions were: nebulizer pressure, 40 psi;  
124 vaporizer temperature, 325 °C; drying gas (N<sub>2</sub>) at 4 L/min and 325 °C;  
125 capillary voltage, 5 kV (positive mode); corona, 4 μA; fragmentor, 170 V and  
126 280 V for the internal standard C<sub>46</sub> (Huguet et al., 2006) and natural  
127 GDGTs, respectively. About 60 *m/z* values (42 of them being reported in

128 Supplementary Table S1) were considered for GDGT detection using SIM  
129 with a dwell time of 16 ms to assess the shapes of GDGT peaks (Fig. 1). The  
130 samples were analyzed five times each. All the analyses were carried out  
131 within a few days after an APCI autotune in positive mode, so the APCI  
132 source and QMS are assumed to be properly calibrated. The QMS was  
133 calibrated by monitoring the  $m/z$  values of four APCI calibration compounds:  
134 121.1, 622.0, 922.0 and 1522.0. Because we considered the correct and  
135 incorrect  $m/z$  values at the same time, the cleanliness and stability  
136 conditions of the APCI source and quadrupole ion optics were not the  
137 limiting factors for our study as confirmed by the coherent and systematic  
138 differences described below.

139 The mass spectra at the apex of each GDGT peak were averaged over  
140 the five replicates of the five selected samples and then normalized to 100%  
141 (Fig. 1; Supplementary Table S1). The 5-, 6- and 7-methyl brGDGT isomers  
142 were treated as separate compounds due to the improved GDGT separation.  
143 The exact BIT values were calculated using equation (1) based on the GDGT  
144 peak areas at the  $m/z$  values of 1292.3, 1050.0, 1036.0 and 1022.0 (after, for  
145 instance, Herfort et al., 2006; Supplementary Table S2).

146 Two unique mass defects were tested: (i) a unique mass defect of 1.0,  
147 which favors brGDGTs over crenarchaeol, and (ii) a unique mass defect of  
148 1.3, which favors crenarchaeol over brGDGTs (Fig. 1). The modified BIT  
149 values using the unique mass defects of 1.0 and 1.3 were calculated using  
150 equation (1) based on the GDGT peak areas at the  $m/z$  values of 1292.0,



151 1050.0, 1036.0 and 1022.0, and at the  $m/z$  values of 1292.3, 1050.3, 1036.3  
152 and 1022.3, respectively (Supplementary Table S2). All single-ion  
153 chromatograms were obtained using  $m/z$  windows restricted to, for instance,  
154 1050.3–1050.3 to extract the ion at  $m/z$  1050.3 only. The shifts in BIT values  
155 were then determined for each unique mass defect and each sample as the  
156 modified BIT values minus the exact BIT values – i.e.,  $\Delta\text{BIT} = \text{Modified BIT}$   
157  $\text{value} - \text{Exact BIT value}$ . Errors on GDGT signals and BIT values were  
158 calculated based on the five replicates per sample and propagated to the  
159 shifts in BIT values using the variance formula. The biases on GDGT  
160 signals and BIT values were assessed with paired Student's  $t$ -tests, which  
161 were considered significant if  $p < 0.05$ .

162

### 163 **3. Results and discussion**

164 Under the two unique mass defect scenarios, the relative losses of  
165 GDGT signals were calculated using the GDGT peak areas (Table 2). A  
166 deviation of 0.2–0.3 Da from the exact molecular mass generated losses of  
167 relative GDGT signals between 35 and 36% for crenarchaeol, and between  
168 18 and 27% for brGDGTs (Table 2; all paired Student's  $t$ -tests on GDGT  
169 peak areas with  $p < 0.01$ ). Therefore, for any given sample processing  
170 technique, chromatographic method, properly calibrated MS, mass setting  
171 and MS technique (e.g., Escala et al., 2009; Schouten et al., 2009, 2013), not  
172 taking into account the mass defect difference between crenarchaeol and  
173 brGDGTs is indeed sufficient to obtain different GDGT relative responses

174 and thus different BIT values. It is noteworthy that this caveat applies not  
175 only to the BIT index (Fig. 2; Table 3), but also to all GDGT-based indices  
176 that consider both isoprenoid GDGTs and brGDGTs.

177 Shifts in BIT values varied between 0.013 and 0.093 using a unique  
178 mass defect of 1.0, and between  $-0.055$  and  $-0.011$  using a unique mass  
179 defect of 1.3 (Fig. 2; Table 3; all paired Student's *t*-tests on BIT values with  
180  $p < 0.01$ ). Under both unique mass defect scenarios, the highest shifts in  
181 BIT values occurred for the sediment samples from the core MD04-2790,  
182 which also had intermediate BIT values (Fig. 2; Table 3). Our results are  
183 consistent with those from the two round-robin GDGT studies, which gave  
184 higher BIT index scatter for samples with intermediate BIT values than  
185 they did for samples with extreme BIT values (Schouten et al., 2009, 2013a).  
186 Theoretically, the observed shifts in BIT values are explained by a reduction  
187 by 35% of the relative crenarchaeol signal using the unique mass defect of  
188 1.0, and by a general reduction by 21% of the relative brGDGT signal using  
189 the unique mass defect of 1.3 (Fig. 2).

190 To assess the severity of the observed and estimated shifts in BIT  
191 values due to approximate mass selection, these shifts are compared with  
192 the 95% confidence intervals of interlaboratory means for single QMS only  
193 based on the latest round-robin GDGT study (Schouten et al., 2013a). The  
194 observed biases on BIT values for the five selected sediment samples were  
195 generally larger than the interlaboratory scatter of the relevant round-robin  
196 samples for single QMS only (Fig. 2). The observed biases on BIT values are

197 also not negligible compared to the interlaboratory scatter for all MS types  
198 (Schouten et al., 2013a). This suggests that approximate mass selection  
199 probably contributes to interlaboratory differences.

200        Laboratories 16, 18, 23 and 25 summed  $[M+H]^+$  and  $[M+H+1]^+$  ions –  
201 protonated molecule and first isotope peak with one  $^{13}\text{C}$  atom – for BIT  
202 index calculations instead of  $[M+H]^+$  ions only during the latest round-robin  
203 GDGT study (Schouten et al., 2013a), which leads to another bias due to the  
204 various numbers of carbon atoms between the different GDGTs. To assess  
205 this bias, the abundances of  $[M+H+1]^+$  ions relative to  $[M+H]^+$  ions were  
206 calculated for the GDGTs included in the BIT index (Table 1) and then used  
207 to theoretically estimate the shifts in BIT values depending on the initial  
208 BIT index value. The calculated shifts reach a maximal value of  $-0.03$  for an  
209 initial BIT index value close to 0.5 (Fig. 2), which means that the most likely  
210 sources of bias in addition to approximate mass selection are, among others,  
211 the diversity of APCI parameters and MS types (e.g., Escala et al., 2009;  
212 Schouten et al., 2009, 2013).

213

#### 214 4.        **Conclusions and perspectives**

215        The results obtained from five sediment samples showed that not  
216 taking into account the systematic mass defect difference between  
217 crenarchaeol and brGDGTs generated shifts in BIT values of up to  $\pm 0.1$  unit.  
218 The observed shifts in BIT values represent a non-negligible proportion of  
219 the interlaboratory scatter. A round-robin GDGT study focusing on mass

220 selection for SIM experiments would greatly help to assess the contribution  
221 of approximate mass selection to the interlaboratory scatter of BIT values.

222

## 223 **Acknowledgements**

224 Work at CEREGE is supported by the Collège de France and BNP-  
225 Paribas Foundation (project CPATEMP). N.D. expresses her thanks to the  
226 Ecole Normale Supérieure de Lyon for providing PhD salary support. The  
227 authors thank the reviewers of an earlier version of this paper.

228

## 229 **Appendix A. Supplementary material**

230

231 *Associate Editor*—**Ann Pearson**

232

## 233 **References**

234 Basse, A., Zhu, C., Versteegh, G.J.M., Fischer, G., Hinrichs, K.-U.,  
235 Mollenhauer, G., 2014. Distribution of intact and core tetraether  
236 lipids in water column profiles of suspended particulate matter off  
237 Cape Blanc, NW Africa. *Organic Geochemistry* 72, 1–13.

238 Cao, J., Rao, Z., Jia, G., Xu, Q., Chen, F., 2017. A 15 ka pH record from an  
239 alpine lake in north China derived from the cyclization ratio index of  
240 aquatic brGDGTs and its paleoclimatic significance. *Organic*  
241 *Geochemistry* 109, 31–46.

242 De Jonge, C., Hopmans, E.C., Stadnitskaia, A., Rijpstra, W.I.C., Hofland, R.,  
243 Tegelaar, E., Sinninghe Damsté, J.S., 2013. Identification of novel  
244 penta- and hexamethylated branched glycerol dialkyl glycerol  
245 tetraethers in peat using HPLC–MS<sup>2</sup>, GC–MS and GC–SMB-MS.  
246 *Organic Geochemistry* 54, 78–82.

247 Ding, S., Schwab, V.F., Ueberschaar, N., Roth, V.-N., Lange, M., Xu, Y.,  
248 Gleixner, G., Pohnert, G., 2016. Identification of novel 7-methyl and  
249 cyclopentanyl branched glycerol dialkyl glycerol tetraethers in lake  
250 sediments. *Organic Geochemistry* 102, 52–58.

251 Escala, M., Fietz, S., Rueda, G., Rosell-Melé, A., 2009. Analytical  
252 considerations for the use of the paleothermometer Tetraether  
253 Index<sub>86</sub> and the branched vs isoprenoid tetraether index regarding  
254 the choice of cleanup and instrumental conditions. *Analytical*  
255 *Chemistry* 81, 2701–2707.

256 Freymond, C.V., Peterse, F., Fischer, L.V., Filip, F., Giosan, L., Eglinton,  
257 T.I., 2017. Branched GDGT signals in fluvial sediments of the  
258 Danube River basin: method comparison and longitudinal evolution.  
259 *Organic Geochemistry* 103, 88–96.

260 Herfort, L., Schouten, S., Boon, J.P., Sinninghe Damsté, J.S., 2006.  
261 Application of the TEX<sub>86</sub> temperature proxy to the southern North  
262 Sea. *Organic Geochemistry* 37, 1715–1726.

263 Hopmans, E.C., Schouten, S., Pancost, R.D., van der Meer, M.T.J.,  
264 Sinninghe Damsté, J.S., 2000. Analysis of intact tetraether lipids in

265 archaeal cell material and sediments by high performance liquid  
266 chromatography/atmospheric pressure chemical ionization mass  
267 spectrometry. *Rapid Communications in Mass Spectrometry* 14, 585–  
268 589.

269 Hopmans, E.C., Schouten, S., Sinninghe Damsté, J.S., 2016. The effect of  
270 improved chromatography on GDGT-based palaeoproxies. *Organic*  
271 *Geochemistry* 93, 1–6.

272 Hopmans, E.C., Weijers, J.W.H., Schefuß, E., Herfort, L., Sinninghe  
273 Damsté, J.S., Schouten, S., 2004. A novel proxy for terrestrial organic  
274 matter in sediments based on branched and isoprenoid tetraether  
275 lipids. *Earth and Planetary Science Letters* 224, 107–116.

276 Huguet, C., Hopmans, E.C., Febo-Ayala, W., Thompson, D.H., Sinninghe  
277 Damsté, J.S., Schouten, S., 2006. An improved method to determine  
278 the absolute abundance of glycerol dibiphytanyl glycerol tetraether  
279 lipids. *Organic Geochemistry* 37, 1036–1041.

280 Keisling, B.A., Castañeda, I.S., Brigham-Grette, J., 2017. Hydrological and  
281 temperature change in Arctic Siberia during the intensification of  
282 Northern Hemisphere Glaciation. *Earth and Planetary Science*  
283 *Letters* 457, 136–148.

284 Ménot, G., Bard, E., 2012. A precise search for drastic temperature shifts of  
285 the past 40,000 years in southeastern Europe. *Paleoceanography* 27,  
286 PA2210.

287 Naafs, B.D.A., Inglis, G.N., Zheng, Y., Amesbury, M.J., Biester, H., Bindler,  
288 R., Blewett, J., Burrows, M.A., del Castillo Torres, D., Chambers,  
289 F.M., Cohen, A.D., Evershed, R.P., Feakins, S.J., Gałka, M., Gallego-  
290 Sala, A., Gandois, L., Gray, D.M., Hatcher, P.G., Honorio Coronado,  
291 E.N., Hughes, P.D.M., Huguet, A., Könönen, M., Laggoun-Défarge, F.,  
292 Lähteenoja, O., Lamentowicz, M., Marchant, R., McClymont, E.,  
293 Pontevedra-Pombal, X., Ponton, C., Pourmand, A., Rizzuti, A.M.,  
294 Rochefort, L., Schellekens, J., De Vleeschouwer, F., Pancost, R.D.,  
295 2017. Introducing global peat-specific temperature and pH  
296 calibrations based on brGDGT bacterial lipids. *Geochimica et*  
297 *Cosmochimica Acta* 208, 285–301.

298 Ruan, J., Huang, Y., Shi, X., Liu, Y., Xiao, W., Xu, Y., 2017. Holocene  
299 variability in sea surface temperature and sea ice extent in the  
300 northern Bering Sea: a multiple biomarker study. *Organic*  
301 *Geochemistry* 113, 1–9.

302 Sanchi, L., Ménot, G., Bard, E., 2013. An automated purification method for  
303 archaeal and bacterial tetraethers in soils and sediments. *Organic*  
304 *Geochemistry* 54, 83–90.

305 Schouten, S., Hopmans, E.C., Rosell-Melé, A., Pearson, A., Adam, P.,  
306 Bauersachs, T., Bard, E., Bernasconi, S.M., Bianchi, T.S., Brocks,  
307 J.J., Carlson, L.T., Castañeda, I.S., Derenne, S., Selver, A.D., Dutta,  
308 K., Eglinton, T., Fosse, C., Galy, V., Grice, K., Hinrichs, K.-U., Huang,  
309 Y., Huguet, A., Huguet, C., Hurley, S., Ingalls, A., Jia, G., Keely, B.,

310 Knappy, C., Kondo, M., Krishnan, S., Lincoln, S., Lipp, J.,  
311 Mangelsdorf, K., Martínez-García, A., Ménot, G., Mets, A.,  
312 Mollenhauer, G., Ohkouchi, N., Ossebaar, J., Pagani, M., Pancost,  
313 R.D., Pearson, E.J., Peterse, F., Reichart, G.-J., Schaeffer, P.,  
314 Schmitt, G., Schwark, L., Shah, S.R., Smith, R.W., Smittenberg, R.H.,  
315 Summons, R.E., Takano, Y., Talbot, H.M., Taylor, K.W.R., Tarozo, R.,  
316 Uchida, M., van Dongen, B.E., Van Mooy, B.A.S., Wang, J., Warren,  
317 C., Weijers, J.W.H., Werne, J.P., Woltering, M., Xie, S., Yamamoto,  
318 M., Yang, H., Zhang, C.L., Zhang, Y., Zhao, M., Sinninghe Damsté,  
319 J.S., 2013a. An interlaboratory study of TEX<sub>86</sub> and BIT analysis of  
320 sediments, extracts, and standard mixtures. *Geochemistry,*  
321 *Geophysics, Geosystems* 14, 5263–5285.

322 Schouten, S., Hopmans, E.C., Sinninghe Damsté, J.S., 2013b. The organic  
323 geochemistry of glycerol dialkyl glycerol tetraether lipids: a review.  
324 *Organic Geochemistry* 54, 19–61.

325 Schouten, S., Hopmans, E.C., van der Meer, J., Mets, A., Bard, E., Bianchi,  
326 T.S., Diefendorf, A., Escala, M., Freeman, K.H., Furukawa, Y.,  
327 Huguet, C., Ingalls, A., Ménot-Combes, G., Nederbragt, A.J., Oba, M.,  
328 Pearson, A., Pearson, E.J., Rosell-Melé, A., Schaeffer, P., Shah, S.R.,  
329 Shanahan, T.M., Smith, R.W., Smittenberg, R., Talbot, H.M., Uchida,  
330 M., Van Mooy, B.A.S., Yamamoto, M., Zhang, Z., Sinninghe Damsté,  
331 J.S., 2009. An interlaboratory study of TEX<sub>86</sub> and BIT analysis using



332 high-performance liquid chromatography–mass spectrometry.  
333 Geochemistry, Geophysics, Geosystems 10, Q03012.

334 Sinninghe Damsté, J.S., Rijpstra, W.I.C., Hopmans, E.C., Foesel, B.U.,  
335 Wüst, P.K., Overmann, J., Tank, M., Bryant, D.A., Dunfield, P.F.,  
336 Houghton, K., Stott, M.B., 2014. Ether- and ester-bound *iso*-diabolic  
337 acid and other lipids in members of *Acidobacteria* subdivision 4.  
338 Applied and Environmental Microbiology 80, 5207–5218.

339 Sinninghe Damsté, J.S., Rijpstra, W.I.C., Hopmans, E.C., Weijers, J.W.H.,  
340 Foesel, B.U., Overmann, J., Dedysh, S.N., 2011. 13,16-dimethyl  
341 octacosanedioic acid (*iso*-diabolic acid), a common membrane-  
342 spanning lipid of *Acidobacteria* subdivisions 1 and 3. Applied and  
343 Environmental Microbiology 77, 4147–4154.

344 Sinninghe Damsté, J.S., Schouten, S., Hopmans, E.C., Duin, A.C.T. van,  
345 Geenevasen, J.A.J., 2002. Crenarchaeol: the characteristic core  
346 glycerol dibiphytanyl glycerol tetraether membrane lipid of  
347 cosmopolitan pelagic crenarchaeota. Journal of Lipid Research 43,  
348 1641–1651.

349 Weijers, J.W.H., Panoto, E., van Bleijswijk, J., Schouten, S., Rijpstra,  
350 W.I.C., Balk, M., Stams, A.J.M., Sinninghe Damsté, J.S., 2009.  
351 Constraints on the biological source(s) of the orphan branched  
352 tetraether membrane lipids. Geomicrobiology Journal 26, 402–414.

353 Woelders, L., Vellekoop, J., Kroon, D., Smit, J., Casadío, S., Prámparo, M.B.,  
354 Dinarès-Turell, J., Peterse, F., Sluijs, A., Lenaerts, J.T.M., Speijer,

355 R.P., 2017. Latest Cretaceous climatic and environmental change in  
356 the South Atlantic region. *Paleoceanography* 32, 466–483.

357 Yang, H., Ding, W., Zhang, C.L., Wu, X., Ma, X., He, G., Huang, J., Xie, S.,  
358 2011. Occurrence of tetraether lipids in stalagmites: implications for  
359 sources and GDGT-based proxies. *Organic Geochemistry* 42, 108–115.

360

361 **Figure captions**

362 **Fig. 1.** Examples of averaged mass spectra normalized to 100% of (A)  
363 crenarchaeol and of (B) brGDGT-Ia for the sediment sample at 2860 cm  
364 depth in core MD04-2790. The error bars correspond to the standard  
365 deviations ( $\sigma$ ) of the averaged relative GDGT signals per mass (mean value  
366  $\pm 2\sigma$ ,  $n = 5$ ). The blue and brown dashed lines describe the scenarios that  
367 consider a unique mass defect ( $\Delta M$ ) of 1.0 and 1.3, respectively. The black  
368 curves represent the Gaussian functions fitted to the averaged mass spectra  
369 so that the shapes of GDGT peaks are more apparent.

370

371 **Fig. 2.** Shifts in BIT values ( $\Delta BIT$ ) vs exact mass spectrometry-based BIT  
372 values according to the unique mass defect (1.0 or 1.3). The blue and brown  
373 symbols indicate the results from five sediment samples. The horizontal  
374 error bars correspond to the standard deviations ( $\sigma$ ) of the exact BIT values  
375 indicated in Table 3 (mean value  $\pm 2\sigma$ ,  $n = 5$ ). The vertical error bars  
376 correspond to the standard deviations of the  $\Delta BIT$  values, which were  
377 determined by propagating the standard deviations shown in Table 3 using  
378 the variance formula (mean value  $\pm 2\sigma$ ,  $n = 5$ ). The blue and brown solid  
379 curves indicate the theoretical results for given losses of crenarchaeol and  
380 brGDGT signals, respectively. The dark red solid curves indicate the  
381 theoretical results when  $[M+H]^+$  and  $[M+H+1]^+$  ions – protonated molecule  
382 and first isotope peak with one  $^{13}C$  atom, respectively – are summed for BIT  
383 index calculations instead of  $[M+H]^+$  ions only. The colored double arrows

384 indicate the 95% confidence intervals ( $\pm t \times \text{SD}/\sqrt{n}$ , with  $t = 2.12$  the  $t$ -  
385 statistic value for a two-sided 95% confidence interval with 16 degrees of  
386 freedom, SD the standard deviation and  $n = 17$ ) of interlaboratory means for  
387 single quadrupole mass spectrometers only from the latest round-robin  
388 GDGT study (Schouten et al., 2013a). The x-axis positions of the colored  
389 double arrows correspond to the averaged interlaboratory BIT values for  
390 single quadrupole mass spectrometers only.

391

## 392 **Table captions**

### 393 **Table 1**

394 Molecule names, nominal and exact masses of  $[M]^+$  and  $[M+H]^+$  ions – non-  
395 protonated and protonated molecules, respectively – mass defects of  $[M+H]^+$   
396 ions and abundances of  $[M+H+1]^+$  ions – first isotope peak with one  $^{13}\text{C}$   
397 atom – relative to  $[M+H]^+$  ions. The compounds are indicated following the  
398 nomenclature of Ding et al. (2016). All masses and mass defects shown here  
399 assume GDGTs with only  $^{12}\text{C}$ ,  $^1\text{H}$  and  $^{16}\text{O}$  isotopes. Note that the mass  
400 defect is independent of the protonation, which adds about 1 Da to both  
401 nominal and exact molecular masses.

402

### 403 **Table 2**

404 Relative losses of GDGT signals (in %) of five sediment samples using the  
405 unique mass defects of 1.0 and 1.3 for crenarchaeol and brGDGTs,  
406 respectively. The errors correspond to the standard deviations ( $\sigma$ ) per

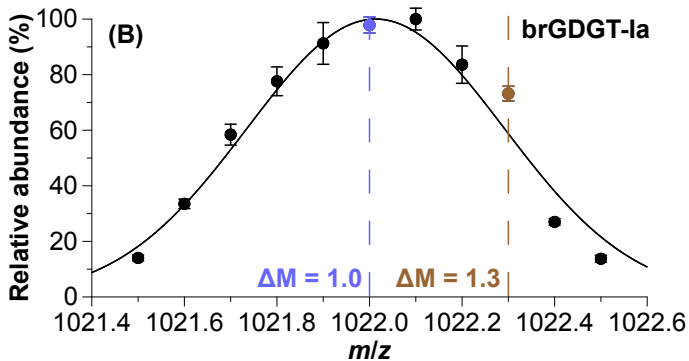
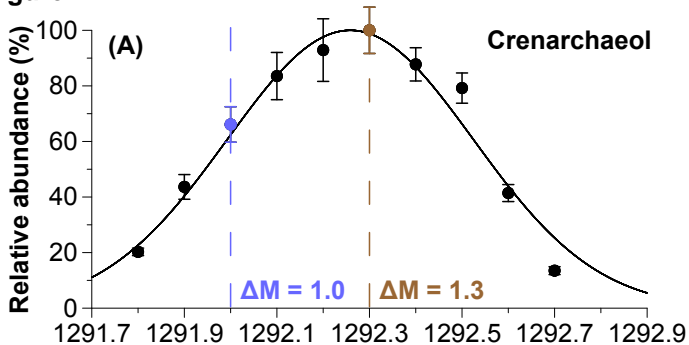
407 compound and per sample (mean value  $\pm 2\sigma$ ,  $n = 5$ ). The compounds are  
408 indicated following the nomenclature of Ding et al. (2016).

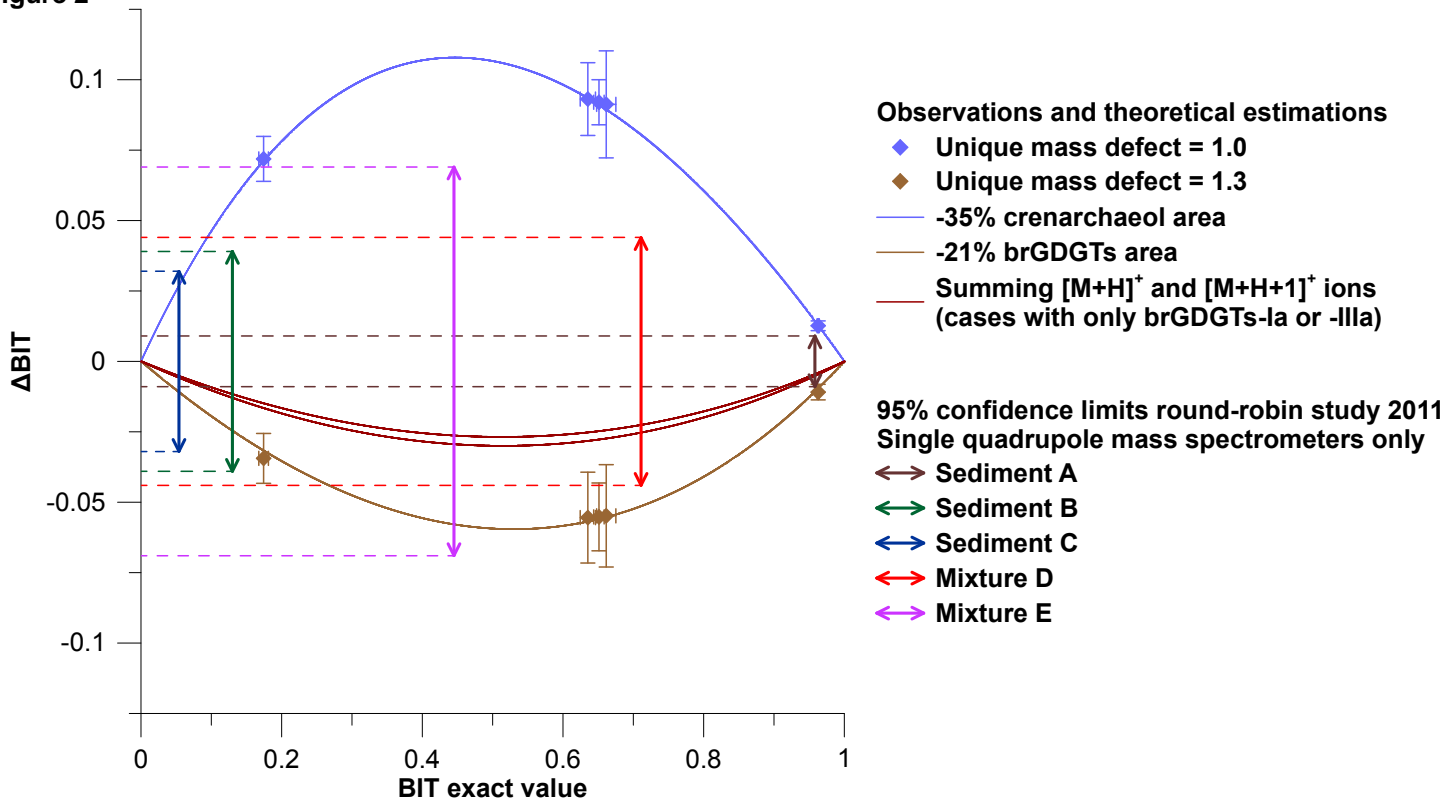
409

410 **Table 3**

411 Exact and modified mass spectrometry-based BIT values of five sediment  
412 samples according to the unique mass defect (1.0 or 1.3). The errors  
413 correspond to the standard deviations ( $\sigma$ ) per scenario and per sample (mean  
414 value  $\pm 2\sigma$ ,  $n = 5$ ).

**Figure 1**



**Figure 2**

**Table 1 - revised**

Molecule name	Nominal mass for [M] <sup>+</sup>	Nominal mass for [M+H] <sup>+</sup>	Exact mass for [M+H] <sup>+</sup>	Mass defect for [M+H] <sup>+</sup>	[M+H+1] <sup>+</sup> /[M+H] <sup>+</sup> ions
Crenarchaeol/Crenarchaeol regio-isomer	1290	1291	1292.2444	1.2444	0.946
brGDGT-IIIa <sub>5</sub> /brGDGT-IIIa <sub>6</sub> /brGDGT-IIIa <sub>7</sub>	1048	1049	1050.0488	1.0488	0.748
brGDGT-IIa <sub>5</sub> /brGDGT-IIa <sub>6</sub> /brGDGT-IIa <sub>7</sub>	1034	1035	1036.0325	1.0325	0.737
brGDGT-Ia	1020	1021	1022.0166	1.0166	0.726



**Table 2**

Sample	Ia	IIa <sub>5</sub>	IIa <sub>6</sub>	IIa <sub>7</sub>	IIIa <sub>5</sub>	IIIa <sub>6</sub>	IIIa <sub>7</sub>	Cren
Bay of Marseille	27 ± 1	24 ± 6	20 ± 5	21 ± 8	20 ± 1	20 ± 4	25 ± 4	35 ± 2
Lake Chad LT17	25 ± 2	21 ± 2	21 ± 4	23 ± 7	20 ± 4	21 ± 2	21 ± 3	35 ± 2
MD04-2790 2851 cm	26 ± 2	21 ± 4	22 ± 2	23 ± 7	19 ± 1	20 ± 2	21 ± 5	36 ± 3
MD04-2790 2860 cm	27 ± 2	22 ± 5	22 ± 4	25 ± 10	19 ± 3	18 ± 4	18 ± 8	35 ± 1
MD04-2790 2870 cm	26 ± 3	22 ± 2	20 ± 2	26 ± 3	19 ± 2	20 ± 4	23 ± 11	35 ± 2

**Table 3**

Sample	Exact value	Unique mass defect = 1.0	Unique mass defect = 1.3
Bay of Marseille	$0.174 \pm 0.007$	$0.246 \pm 0.004$	$0.140 \pm 0.006$
Lake Chad LT17	$0.963 \pm 0.002$	$0.976 \pm 0.001$	$0.952 \pm 0.002$
MD04-2790 2851 cm	$0.661 \pm 0.014$	$0.753 \pm 0.013$	$0.607 \pm 0.012$
MD04-2790 2860 cm	$0.635 \pm 0.011$	$0.728 \pm 0.007$	$0.580 \pm 0.012$
MD04-2790 2870 cm	$0.651 \pm 0.007$	$0.743 \pm 0.003$	$0.596 \pm 0.010$